Proceedings of IMECE'03
2003 ASME International Mechanical Engineering Congress
Washington, D.C., November 15–21, 2003

IMECE2003-41348

ANALYSIS AND DESIGN OF THERMOELECTRIC INFRARED MICROSENSOR

Ke-Min Liao and Rongshun Chen
Department of Power Mechanical Engineering
National Tsing Hua University
Hsinchu 300, TAIWAN, R.O.C.
Email: rchen@pme.nthu.edu.tw

Bruce C. S. Chou
LighTuning Technology Inc.
Hsinchu 300, TAIWAN, R.O.C.
Email: bruce@lightuning.com.tw

ABSTRACT

In this study, a novel thermoelectric infrared microsensor (TIMS) is designed by using commercial CMOS IC processes with subsequent bulk-micromachining process. This microsensor has the advantages of high fill factor, low noise equivalent temperature difference (NETD), and simple fabrication process. The key feature is that thermocouple cantilever beams with low solid thermal conductance have been placed under the membrane of thermoelectric infrared microsensor. In order to improve the performance of the infrared sensor, the basic physical characteristics of this sensor have been analyzed. Finite element analysis is used to simulate the electro-thermo-mechanical behavior of the device and to demonstrate the feasibility of our design. Besides, a method for manufacturing the infrared microsensor is also provided and the performance of the presented design has been examined. The analytical results concluded that lowering down the number of the thermocouples does not affect the responsivity but do reduce the total resistance. Also, the detectivity and responsivity are obviously increased for the proposed TIMS. Finally, the deviation between the theoretical and the simulated results is discussed.

INTRODUCTION

In the last few years, thermoelectric sensors have been widely applied to many areas, such as infrared radiation, temperature, gas flow, or AC power. Thermoelectric infrared microsensors (TIMS) will be very promising if they do not require cooling, have a wide spectral bandwidth response, and are low cost. Most high performance infrared sensors, based on bolometer arrays, have been presented and used so far for thermal imaging in the fields of military detection systems, industrial automation, and home security monitoring [1-8]. These devices, however, are not compatible with the standard IC fabrication methods or generally require vacuum packaging and thermal stabilization. Thus, higher cost of productions and lower sensitivity can be expected.

There are two types of infrared sensors: the thermal type and the quantum type. The thermal type includes contacting temperature sensors, such as the thermocouple and bolometer, and non-contacting pyroelectric sensor. All thermally based infrared sensor convert incident infrared into heat and then into an electric signal. In contrast, the quantum type has strong wavelength dependence and high responsivity with faster responses and includes the photoconductive and photovoltaic devices. Nevertheless, quantum type sensors are limited by their narrow spectral bandwidth and fail to reach far IR region. Thermopile technology is employed in this paper because it does not need an electrical bias during operating and have a DC response as long as the temperature difference is maintained. Thus, it rejects the noise voltage against the power source, which has been a serious disadvantage of other thermal sensors, for example, a bolometer. Moreover, the thermopile sensor does not need a chopper to move the signal of interest away from the very low frequency where 1/f noise is important, whereas pyroelectric sensors do.

The first micromachined thermopile-based linear infrared sensing arrays were reported by Choi and Wise [9]. Each element of such an array consists of a separate thin membrane spanning a silicon rim. The rim acts always as heat sink and results in a negligible cross-talk. In addition, a micromachined 16×16 array of thermoelectric infrared sensors have been fabricated in a commercial CMOS IC process with subsequent bulk-micromachining to show the temperature resolution of 176 mK at 1 Hz framerate [10]. A 1024-element bulk-micromachined thermopile infrared imaging array has been reported for use in automated semiconductor process control with the responsivity of 15 V/W and a thermal time constant of

1ms [11].

This paper reports a novel bulk-micromachined thermoelectric infrared microsensor with the advantages of high fill factor, low noise equivalent temperature difference (NETD), and simple fabrication process. The key feature is that thermocouple cantilever beams with low solid thermal conductance have been placed under the membrane of thermoelectric infrared microsensor. The sensor array is designed using only commercially available industrial CMOS IC fabrication steps. The proposed TIMS may have potentials to be applied in security, fire detection, search and manufacturing. In order to improve the performance of the infrared sensor, the basic physical characteristics of this sensor have been analyzed. Finite element analysis is employed to simulate the electro-thermo-mechanical behavior of the device and to demonstrate the feasibility of our design. The aim of the simulations is to provide the characteristics of variables for the device, which may help the designers for choosing better parameters when fabricated. Besides, a method for manufacturing the infrared microsensor is provided and the performance of the presented design has been examined. Finally, the deviation between the theoretical and the simulated results is discussed.

MICROSENSOR DESIGN

Figure 1 is the schematics of the proposed thermoelectric infrared microsensor (TIMS), which includes a substrate, a suspending membrane, and two thermal couples. The thermocouple cantilever beam is constructed by two layers of polysilicons with p-type polysilicon atop n-type polysilicon. The suspending membrane is supported by two thermocouple cantilever beams, formed above the substrate with a first end and a second end. The first end connects to the substrate to form a cold junction, while the second end is attached to the suspending membrane to form a hot junction. The integrated circuit can be fabricated in the substrate to perform the predetermined processing. As a result, the advantages of a fully integrated system become available, the size of the complete sensor system can be reduced, and the reliability of the device is increased.

In this design, the thermopile cantilever beam is covered by the suspending membrane and a black absorber is provided on the suspending membrane for absorbing thermal radiation. By heating the hot junction between the membrane and the cantilever beam, the temperature difference between the hot and cold junctions is produced, thereby generating the diffusion current. A reverse electromotive force is then generated to compensate the diffusion current. The temperature difference between two ends of the thermocouple can be obtained by measuring the Seebeck voltage, whose value is determined from the product of temperature difference between two ends of the thermocouple and the Seebeck coefficients (also called the thermoelectric power) of the p-type and n-type polysilicons of the cantilever beam. Usually, the thermally generated voltage, Seebeck voltage, can be increased by connecting several pairs of thermocouples in series to form a thermopile. Accordingly, the small-signal Seebeck voltage of the thermopile for a given

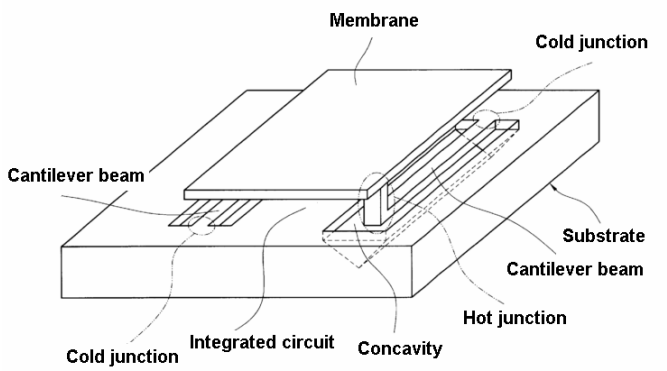

Figure 1 Schematics of the proposed thermoelectric infrared microsensor.

temperature is given by

$$\Delta V = N(\alpha_1 - \alpha_2)\Delta T \tag{1}$$

where N is the number of thermocouple pairs in the thermopile, α_1, α_2 are the Seebeck coefficient of the p-type and n-type polysilicons respectively, and ΔT is the temperature difference across the thermocouples.

SYSTEM CHARACTERIZATION

In order to improve the performance of the infrared sensor, the basic physical characteristics of this sensor are analyzed. Several figures of merits, such as noise equivalent temperature difference (NETD), responsivity R_v, and temperature coefficient of resistance (TCR), are used to characterize the microsensor. NETD is defined as the change in temperature of the object that will cause the signal-to-noise ratio at the output of the thermopile sensor and its read-out circuit to change by unity. NETD is one of the important factors and is requested as small as possible for an infrared sensor. In an idealized situation, we assume that no optical absorption by the delivery medium and the optical system. Thus, NETD can be expressed as

$$NETD = \frac{4F^2 V_n}{R_V A_s L} = \frac{4F^2}{A_s L} NEP \tag{2}$$

where A_s is the effective absorbing area of thermal radiation on the thermopile sensor, V_n is the total noise voltage within the system, F is the focal ratio of the system, NEP = V_n/R_V is the noise equivalent power, and L is the change in power, radiated by the object, per unit area within a spectral band. The noise voltage contains the background noise, the temperature fluctuation noise, and the noise generated by the thermometer, which is made up of Johnson noise and 1/f-noise. Here, the total noise voltage is dominated by the Johnson noise, and is represented by

$$V_n = \sqrt{4kT_s R\Delta f} \tag{3}$$

where k is the Boltzman constant, T_s is the temperature of the thermopile sensor, R is the resistance of the thermocouple, and Δf is the system bandwidth. Responsivity is the amount of output seen per watt of input radiant optical power, and can be written as

$$R_V = \frac{\eta N(\alpha_1 - \alpha_2)}{G_t} \tag{4}$$

where η is the absorption of the incident radiation, and G_t is the total thermal conductance to the substrate. G_t is given by

$$G_t = G_s + G_g + G_r \tag{5}$$

where G_s, G_g, G_r are the solid, gas, and radiation thermal conductance of the infrared sensor respectively. In a more realistic condition, a thermoelectric infrared sensor is usually packaged in a vacuum environment to enhance its performance, thus the gas conductance G_s can be neglected. G_r is also negligible since the operating temperature is not too high to produce the radiative heat, based on the assumption made by Choi and Wise [9]. In this paper only conductive heat flow is needed to be considered and thus Equation (4) can be rewritten as

$$R_V = \frac{\eta N(\alpha_1 - \alpha_2)}{G_s} \tag{6}$$

Moreover, the total solid conductance G_s can be averaged and is equivalent to the sum of a solid conductance G_{Single} of a single thermocouple; that is, $G_s = NG_{Single}$. Therefore, Equation (6) is simplified as

$$R_V = \frac{\eta(\alpha_1 - \alpha_2)}{G_{Single}} \tag{7}$$

Equation (7) is significant since responsivity is simply determined by the characteristics of a single thermocouple: Seebeck coefficients, solid conductance, and absorption of incident radiation. To maximize the responsivity, the absorptivity of hot region should be maximized, and the difference between the thermoelectric powers should be as large as possible. The advantage of this design is that reducing the number of the thermocouples does not affect the responsivity (See Equation (7)), contrasting to the previous designs in the literature, while it decreases the total resistance R. Therefore, the Johnson noise voltage can be reduced and a relatively low NEP is obtained.

It is obvious that reducing the solid thermal conductance by changing the shapes of the thermocouple cantilever beams can increase the responsivity of the sensor. Furthermore, the fill factor of a two-dimensional sensors array, defined as the ratio between a sensor area and a pixel area, is considered. The presented design has a high fill factor due to less space occupied by a fewer number of thermocouples. Therefore, a denser sensors array (more pixels) can be obtained when fixing the chip size. In summary, the presented TIMS has a low NEP and a high fill factor compared with those of previous works.

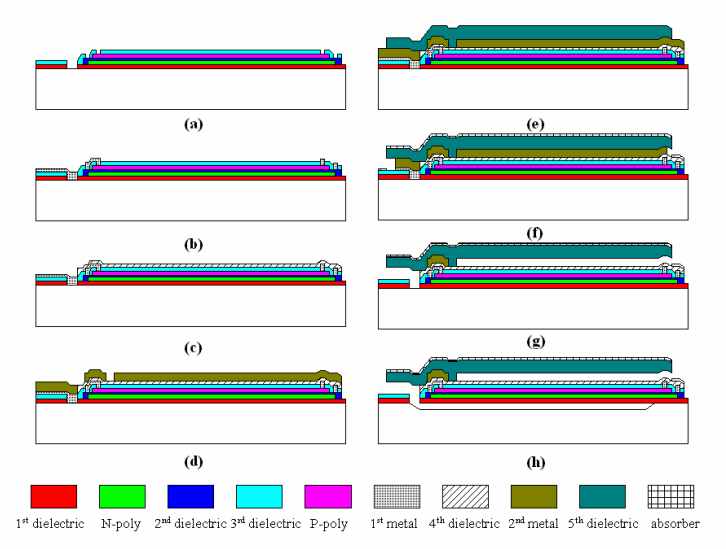

Figure 2 Mirco-fabrication processes

FABRICATION

A method for manufacturing the proposed infrared microsensor by using commercial CMOS IC (0.5 μm 2-poly 2-metal) processes with subsequent bulk-micromachining process is provided. The high reliability of industrial CMOS fabrication processes leads to inexpensive batch-fabrication of the proposed infrared sensor. The fabrication processes are illustrated in Figure 2 and described as follows.

(a) A first dielectric layer, an n-type polysilicon conductor, a second dielectric layer, a p-type polysilicon conductor, and a third dielectric layer are deposited and patterned on the substrate. Wiring via hole then penetrates the dielectric layer to expose parts of the substrate, the n-type polysilicon and the p-type polysilicon.

(b) A first metal wiring layer is subsequently deposited to fill the via hole and to electrically connect p-type polysilicon and n-type polysilicon.

(c) The fourth dielectric layer is deposited and a predetermined portion is removed.

(d) A second metal wiring layer is deposited and patterned to form the sacrificial layer. Part of the metal layer is removed to form a via hole.

(e) The dielectric layer is consequently deposited on the second metal wiring layer and is patterned to define the suspending membrane.

(f) Then, a black absorber (gold black, platinum black, or Ni-Cr) having a thickness of tens to hundreds of angstroms is

formed by a self-deposition technology.

(g) The metal wiring layers are etched from the undercuts to form a first gap and to expose the via hole.

(h) Finally, parts of the substrate under the thermocouple are removed by using the anisotropic etching technology (TMAH) to form a second gap and a suspending cantilever beam structure.

OPTIMIZATION

The geometrical design of the sensor should be optimized by taking into account the thermoelectric and material parameters. As for the sensors array, the suspending membrane area is 49×49 μm^2, the pixel area is 50×50 μm^2, and thus the fill factor is 95%. The thermocouple materials are an n-type polysilicon with a resistance coefficient of 45 μΩ-m and a thermoelectric power of 240 μV/K, and a p-type polysilicon with a resistance coefficient of 100 μΩ-m and a thermoelectric power of 260 μV/K. For the thermocouple cantilever beams, assume the width of the n-type and p-type polysilicons is 0.5 μm, the thickness is 0.3 μm, and the number of thermocouples is N = 2. Moreover, at room temperature and in a vacuum condition, the focal ratio F is unity, the absorption η is 0.85, and Δf is 1 Hz. Under the above assumptions, the NETD against the length of the thermocouple cantilever beam is illustrated in Figure 3. From this figure, it is obvious that the best NETD is 0.003229℃ under different lengths of the thermocouple cantilever beam. Consequently, an optimum length can be chosen. Figure 4 shows the calculated responsivity for the designed infrared sensors for different lengths and areas of a single thermocouple. It can conclude that the area of the thermocouple should be as small as possible for obtaining higher responsivity. The value of theoretical NETD and responsivity R_v versus total thermal conductance G_t is shown in Figure 5, in which the left vertical axis represents the responsivity, while the right vertical axis represents NETD. The responsivity increases as thermal conductivity becomes smaller. The optimal thermal conductance under the above condition is about 5×10^{-8} W/K, R_v is 18,000 V/W.

In addition to the parameters mentioned above, the widths w_1 and w_2, the width of the n-type and p-type polysilicon respectively, can be optimized. Figure 6 shows the calculated NEP as a function of the w_1 and w_2. As shown in the figure, the optimum value is achieved with the thermocouples having minimum sizes. Nevertheless, the optimum NEP is obtained with other sizes of the thermocouple in our calculations while different system parameters are applied. These results demonstrate that individual optimization of the system parameters does not lead to the overall optimum. Thus, entire system has to be taken into account for optimization. When manufacturing the sensor, in practice the length of the thermocouple cantilever is set to 100 μm, and the thermal conductance is about 8.5×10^{-8} W/K. The physical constants and the performance characteristics are summarized in Table 1. The theoretically NETD is 0.0035℃. However, this value is far less than any ever-reported results including a bolometric and pyroelectric sensor in previous literatures.

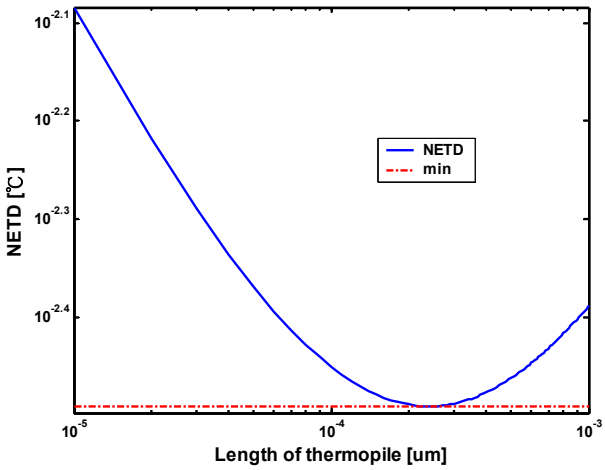

Figure 3 NETD under different length of the thermopile

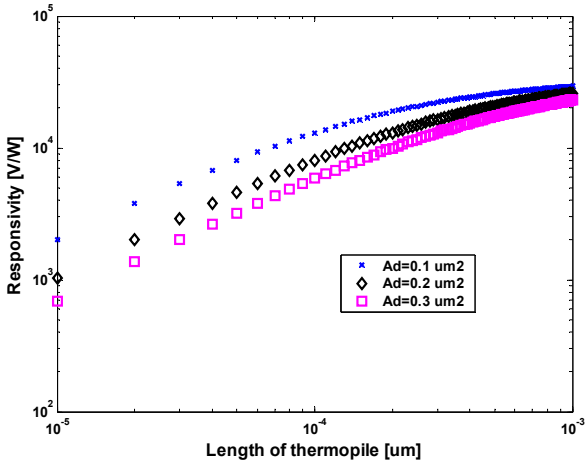

Figure 4 Calculated responsivity for different lengths and areas of single thermocouple

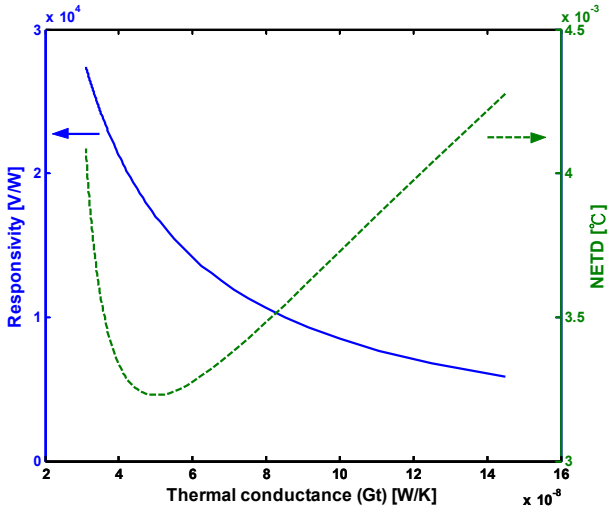

Figure 5 Theoretical NETD and responsivity R_v versus total thermal conductance G_t

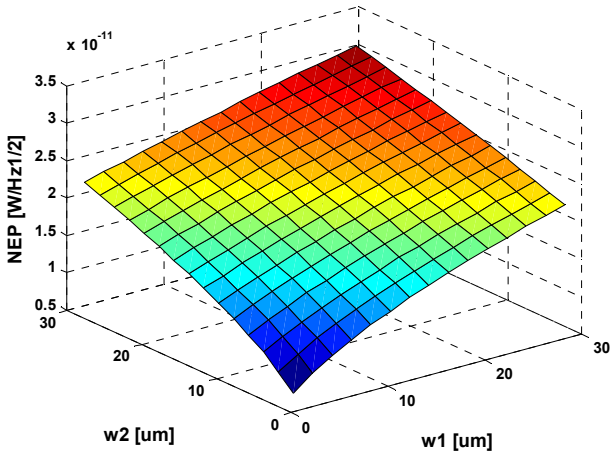

Figure 6 Calculated NEP for different w_1 and w_2

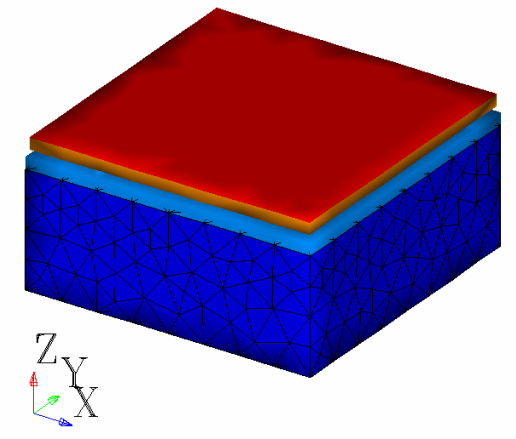

Figure 7 Model of a single pixel microsensor

Table 1 Summary of sensor's properties

Parameters	Value
Single pixel area (μm^2)	50×50
Active area (μm^2)	49×49
Length of a single thermopile (μm)	100
Absorption (%)	85
Fill factor (%)	95
Resistance at 300 K (Ω)	$1.9333\times10^{+5}$
Thermal Conductance (W/K)	8.5×10^{-8}
Responsivity (V/W)	1×10^{4}
NETD at 1Hz framerate (K)	0.0035
NEP at 1Hz pixel rate ($W/Hz^{1/2}$)	5.6583×10^{-12}
Detectivity ($cm\ Hz^{1/2}/W$)	$8.6599\times10^{+8}$
Total noise voltage ($V/Hz^{1/2}$)	5.6583×10^{-8}

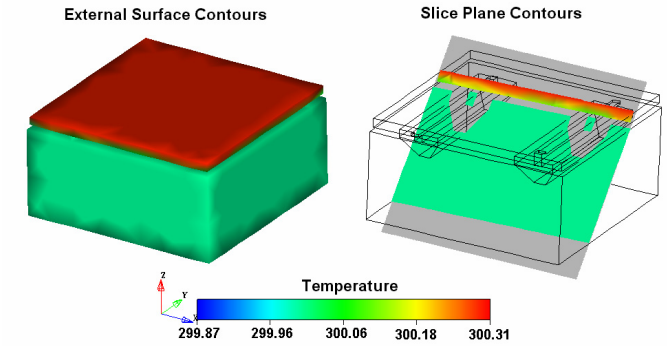

Figure 8 Thermal simulation results: (a) temperature contours of the external surface (b) temperature contours of the slice plane.

FINITE ELEMENT MODELLING

The commercial software CoventorWare is utilized to perform the thermal simulation, including the spatial and temporal temperature distributions of the presented infrared microsensor, at which constant heat loads (100 W/m^2) are applied in the membrane. The task of thermal simulation is to obtain the adequate geometry, sizes, and thermal parameters of the sensor. The appropriate initial and boundary conditions, which describe the integration of the sensor in the physical environment, are also determined in the simulations. The FEM establishes the temperature distribution by dividing the microsensor into a finite number of discrete elements and applying the governing heat balance equations to each element. Once the temperature distribution is simulated, the essential parameters of the designed infrared sensor, such as responsivity or time constant can be easily deduced. The model of a single pixel microsensor is illustrated in Figure 7. In this simulation a constant power is assumed to be absorbed by the sensor core element. The substrate is regarded as heat sinks at sensor temperature T_s. Figure 8 shows the thermal simulation results for the thermopile infrared microsensor. The stationary 3-D temperature distribution in the modeling region is depicted in Figure 8 (a), in which the temperature in the membrane is constant and increases to 300.31 K from 299.97 K in steady state. It demonstrates that the infrared radiation has been absorbed by the membrane with the maximum value at the center of the area. In order to view the temperature profiles below the membrane, the slice plane contours are shown in Figure 8 (b). The 1-D temperature distribution is extracted and presented in Figure (9) for x = 8 μm and y = 25 μm. Thus, the signal gradient for the loaded pixel ΔT can be obtained from this figure. After the signal gradient is derived, the signal voltage and responsivity can be calculated. Here, the length of the thermopile is set to be 40 μm at a pixel irradiance of 100 W/m^2. The simulated responsivity for the single pixel sensor is about 2100 V/W, resulting in 44% deviation, comparing to the value 3800 V/W, derived from the theoretical model with the same length of cantilever beam. The difference between the theoretical model and simulation results is partially that the

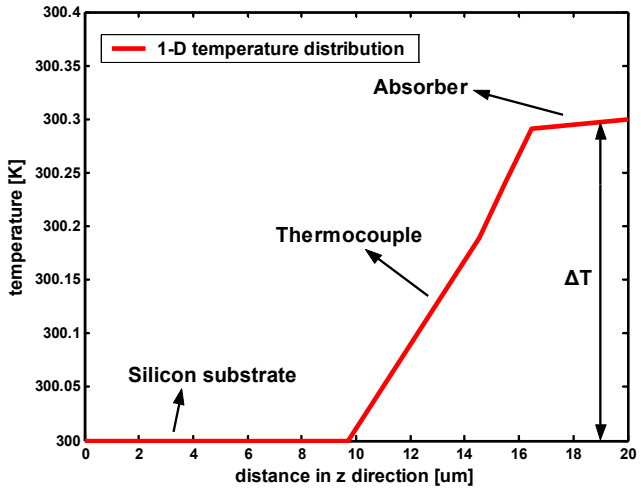

Figure 9 1-D stationary temperature distributions along a line connecting substrate and absorber

vacuum condition was not implemented in the software to reduce the thermal conduction and environmental perturbation in simulations. However if the vacuum condition is applied, higher signal gradient is derived to increase the responsivity of the microsensor. Therefore, vacuum packaging is essential for realizing a high performance thermopile infrared sensor [12]. Furthermore, the thermal time constant can be derived by using transient FEM simulation that gives the temporal dependence of the temperature for each node of the element. The time constant is simulated and is found to be 28 msec.

CONCLUSION

A novel thermoelectric infrared microsensor with the advantages of high fill factor, low NETD, and simple fabrication process is designed and analyzed. The sensor array is designed using commercially available industrial CMOS IC and bulk-micromachined fabrication processes to reduce the cost. To increase the responsivity and fill factor, thermocouple cantilever beams with low solid thermal conductance are placed under the membrane of thermoelectric infrared microsensor. Optimized design parameters of infrared sensor with respect to the output of the microsystem have been discussed. The FEM is utilized to perform the thermal simulation, including the spatial and temporal temperature distributions of the presented infrared microsensor. The simulated responsivity results in 44% deviation, comparing to the theoretical model, due to lacking the vacuum condition in the software. Furthermore, the thermal time constant is found to be 28 msec for the sensor.

ACKNOWLEDGMENT

The authors would like to express their appreciation to the National Center for High-performance Computing (NCHC) for the supporting of the software and equipment.

REFERENCES

[1] Kruse, P., Dodson, R., Anderson, S., Kantor, L., Knipfer M., McManus, T., Wood, A., and Rezachek, T., 1998, "Infrared imager employing 160×120 pixel uncooled bolometer array," *Proc. SPIE Infrared Technology and Applications XXIV*, Vol. 2, pp. 572–577.

[2] Jahanzeb, A., Travers, C. M., Çelik-Butler, Z., Butler, D. P., and Tan, S., 1997, "A semiconductor YBaCuO microbolometer for room temperature IRimaging," *IEEE Trans. Electron Devices*, **44**, pp. 1795–1801.

[3] Almasri, M., Butler, D. P., and Çelik-Butler, Z., 2001, "Self-supporting infrared microbolometers with low-thermal mass," *J. Microelectromech. Syst.*, **10**, pp. 469–476.

[4] Radford, W., Wyles, R., Wyles, J., Varesi, J., Ray, M., Murphy, D., Kennedy, A., Finch, A., Moody, E., Cheung, F., Coda, R., and Baur, S., 1998, "Microbolometer uncooled infrared camera with 20 mK NETD," *Proc. SPIE Infrared Technology and Applications XXIV*, Vol. 3436, pp. 636–646.

[5] Lang, W., and Kühl, K., 1990, "A thin film bolometer for radiation thermometry at ambient temperature," *Sens. Actuators, Phys. A*, **21–23**, pp. 473–477.

[6] Wood, R. A., and Foss, N. A., 1993, "Micromachined bolometer arrays achieve low-cost imaging," *Laser Focus World*, pp. 101–106.

[7] Radford, W., Murphy, D., Ray, M., Propst, S., Kennedy, A., Kojiro, J., Woolaway, J., Soch, K., Coda, R., Lung, G., Moody, E., Gleichman, D., and Baur, S., 1996, "320×240 silicon microbolometer uncooled IRFPA's with on-chip offset correction," *Proc. SPIE Infrared Detectors and Focal Plane Arrays IV*, Vol. 2746, pp. 82–92.

[8] Gray, J. E., Çelik-Butler, Z., Butler, D. P., and Jahanzeb, A., 1998, "Uncooled infrared microbolometers and pyroelectric detectors using semiconducting YBaCuO," *Proc. SPIE Infrared Technology and its Applications XXIV*, Vol. 3436, pp. 555–563.

[9] Choi, I. H., Wise, A., 1986, "A silicon-thermopile-based infrared sensing array for use in automated manufacturing," *IEEE Trans. On Electron Devices*, pp. 72–79.

[10] Schaufelbuehl, A., Munch, U., Menolfi, C., Brand, O., Paul, O., Huang, Q., and Baltes, H., 2001, "256-Pixel CMOS-Integrated Thermoelectric Infrared Sensor Array," *Proc. MEMS (2001)*, pp. 200–203.

[11] Oliver, A. D., and Wise, K. D., 1999, "A 1024-Element Bulk- Micromachined Thermopile Infrared Imaging Array," *Sensors and Actuators A*, **73**, pp. 222–231.

[12] Dillner, U., 1998, "Thermal Simulation and Realization of Micromachined Thermal Sensor Arrays," *Proc. 5th NEXUSPAN Workshop on Thermal Aspects in Microsystem Technology*, pp. 133-141.